

# Quadrupolar Ordering in $\text{LaMnO}_3$ Revealed from Scattering Data and Geometric Modeling

A. Sartbaeva, S. A. Wells, and M. F. Thorpe

*Department of Physics and Astronomy, Arizona State University, Tempe, Arizona 85287-1504, USA*

E. S. Božin and S. J. L. Billinge

*Department of Physics and Astronomy, Michigan State University, East Lansing, Michigan 48824-2320, USA*

(Received 1 May 2007; published 10 October 2007)

Many strongly correlated materials display quadrupolar (Jahn-Teller) distortion of the local octahedral structural units. It is common for these distortions to be observed by probes of local structure but absent in the crystallographic average structure. The ordering of these quadrupoles is important in determining the properties of manganites and cuprates, and the nature of the disorder in these structures has been an unsolved problem. We combine high resolution scattering data and novel geometrical modeling techniques to obtain a detailed picture of the local atomic structure, and also to extract the quadrupolar order parameter associated with the distorted octahedra. We show that in  $\text{LaMnO}_3$ , quadrupoles undergo a strong first-order phase transition at 730 K, but with nonzero order parameter remaining in the high-temperature phase.

DOI: [10.1103/PhysRevLett.99.155503](https://doi.org/10.1103/PhysRevLett.99.155503)

PACS numbers: 61.43.Bn, 61.50.Ah, 71.70.Ej, 75.40.Mg

Extracting detailed structural information from solids that have both long-range order (Bragg peaks) and local disorder (diffuse scattering) is one of the most challenging problems in characterizing complex materials [1]. Here we show how it is possible to combine high resolution neutron scattering data out to large scattering wave vectors, with modeling that preserves the local stereochemistry. The latter requires the introduction of various penalty functions for distortions from perfect crystallinity and is done by a new technique involving geometrical simulation that we have developed. This new combined experiment and modeling approach is illustrated here with  $\text{LaMnO}_3$  where the  $\text{MnO}_6$  octahedra can distort uniaxially and arrange themselves in a quadrupolar ordering pattern.

In manganite perovskites and layered cuprates [2–5], strong Jahn-Teller (JT) coupling [5–12] gives rise to a variety of interesting magnetic, electronic, and structural phenomena such as charge and orbital ordering, ferromagnetism, phase separation, and of course colossal magnetoresistance (CMR) [2–4,13,14] and superconductivity [15,16]. In the undoped end member  $\text{LaMnO}_3$ , crystallographic methods indicate that above about 730 K, the JT distortion ceases to exist [17–19]. The transition is characterized as first order based on the observation of a coexistence of the low and high temperature phases over a range of temperatures and an anomalous volume collapse is observed [19]. However, studies sensitive to local structure [20–22] indicate that locally the octahedra remain JT distorted above the transition and only disappear on average. Although  $\text{LaMnO}_3$  has been investigated using experimental techniques including neutron diffraction [17], transport and SQUID [22], XANES, and EXAFS [21], all of which have led to important insights, none of these has led to a comprehensive structural model or a full description of the nature of the JT phase transition. Here, we have

been successful in combining pair distribution function (PDF) data [20] with new geometrical modeling techniques [23,24] to describe both the short- and long-range order at all temperatures, and most importantly to extract the quadrupolar order parameter. Surprisingly, weak long-range quadrupolar ordering persists above the first-order phase transition at around 730 K up to the highest temperatures studied (1150 K).

Qiu *et al.* [20] studied  $\text{LaMnO}_3$  using data collected at the NPDF diffractometer at Los Alamos National Laboratory. Structural parameters were initially refined using PDFFIT [25]. Models were refined for the data over different length scales  $r$ . Fits confined to the low- $r$  region yielded the local (JT-distorted) structure, whereas fits over wider ranges of  $r$  gradually crossed over to the average crystallographic structures, suggesting that the nature of the high-temperature state is that of orientationally disordered, JT-distorted, octahedra with a short-range local ordering persisting at all temperatures.

To obtain more complete structural models of  $\text{LaMnO}_3$  that fully reconcile the local and the average structures we represent the structure with a large supercell. For each temperature point our starting model was a  $16 \times 16 \times 12$  supercell of the PDF-refined crystal structure, with cell edges of about 90 Å, containing 61 440 atoms (12 288 octahedra). We then refined the atomic positions within this supercell so as to fit its PDF to the experimental PDF, using a simulated-annealing algorithm. In each round of the algorithm, a randomly selected atom is moved, the  $G(r)$  of the new structure is calculated and compared to the experimental  $G(r)$ , and changes that improve the fit are accepted, while those that worsen the fit are accepted or rejected based on a Metropolis criterion. We perform simulated annealing by gradually lowering the pseudotemperature in the Metropolis criterion.

In practice, fitting based only on  $G(r)$  can give unphysical results [26] and some form of constraint must be used to ensure that local chemical bonding and steric exclusion are properly maintained. It is usual to apply harmonic constraints [26] to bond lengths and angles, so that the cost function includes not only the mismatch between experimental and simulated  $G(r)$ , but also the cost of stretching constraints. However, this approach can be used only if equilibrium values for bond lengths are known; since the pattern of JT distortions in the high-temperature structures is not known, we cannot define ideal Mn-O bond lengths in advance.

We have made use of a new form of geometric constraint based on the technique of geometric modeling [23,24,27,28], where the constraints in a bonded group of atoms (here, an  $\text{MnO}_6$  unit) are represented using a rigid “template” which has the ideal geometry of the group. The template may be a regular octahedron or a JT-distorted octahedron with long Mn-O bond of 2.16 Å and a short bond of 1.94 Å [23]. The template shape is chosen based on the aspect ratio of the Mn-O bonds, allowing a JT distortion to develop to fit the data. The application of these templates is shown in Fig. 1. Every time an atom is moved, the template is fitted over the atoms of the group. The distortion of the group from the template geometry is measured by the mismatch of O atoms from template vertices. If the mismatch exceeds a defined tolerance, the move is immediately rejected for violation of bonding geometry. We allowed a tolerance of 0.3 Å, to allow for normal thermal variation in the bond lengths. Conformers

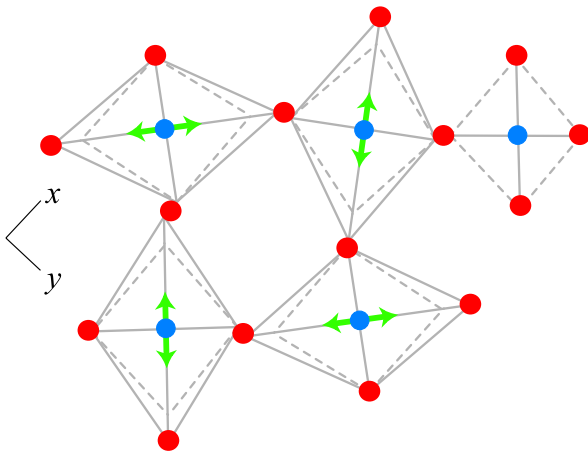
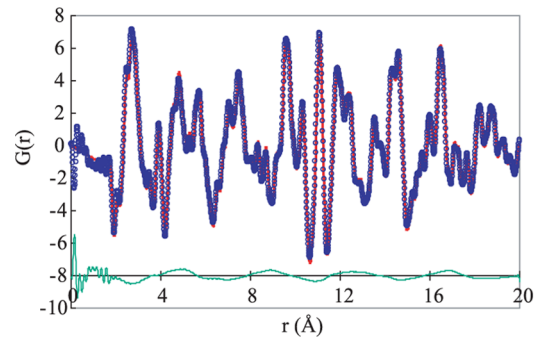


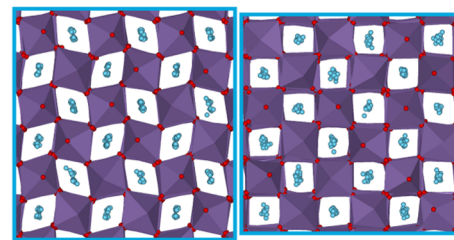
FIG. 1 (color online). Schematic representation of the structure of  $\text{LaMnO}_3$  in the  $xy$  plane showing the checkerboard arrangement of JT-distorted octahedra in the  $xy$  plane with long and short bonds; the direction of JT distortion is emphasized by green (light gray) arrows. A regular octahedron is shown on the right and has all short bonds. Mn ions are in the middle of octahedra, and O ions are at the vertices of octahedra. La atoms are omitted for clarity. Ideal geometric templates for JT-distorted octahedra (gray lines) are superimposed over each octahedron.

are also rejected if two atoms are unacceptably close to each other, e.g., a severe steric clash between an interstitial La and an O atom. If the system passes these geometric tests, the simulated-annealing algorithm then determines whether to accept or reject the move based on its fit to the data.

In Fig. 2(a) we show the PDF  $G(r)$  at 300 K and fit to data. It is notable that we fit both the long-range data and the short-range data (showing splitting of the first Mn-O peak due to the JT distortion) equally well. The fits are comparably good at all temperatures. The width of a peak indicates a distribution of interatomic distances in the model. In Fig. 2(b), we show portions of the fitted structures at 300 and 1050 K. The JT distortion of an octahedron is a quadrupolar (rather than dipolar) distortion, described by a quadrupole moment  $q$ . We analyzed our structures by obtaining the quadrupole moment of each octahedron. The five components of  $q$  are defined in terms of the components  $x, y, z$  of the six Mn-O bond vectors in each octahedron, as follows:



(a)



(b)

FIG. 2 (color online). (a) Representative fit of  $G(r)$  [red (or dark gray) line] to the data [blue (or gray) circles] for  $\text{LaMnO}_3$  at 300 K. The difference is offset below in green (or light gray). (b) Slices of the fitted models for 300 and 1050 K showing arrangement of  $\text{MnO}_6$  octahedra. La ions (light gray or cyan) are interstitial atoms in the channels. At 300 K, there is a checkerboard arrangement of octahedra and La ions are relatively ordered in the channels. At 1050 K—the average structure appears cubiclike, the octahedra are very buckled and La ions are disordered in the channels. The different sizes of the images are due to a small degree of negative thermal expansion [19].

$$\begin{aligned}
 q_1 &= 2 \sum_{i=1}^6 x_i y_i; & q_2 &= 2 \sum_{i=1}^6 y_i z_i; & q_3 &= 2 \sum_{i=1}^6 z_i x_i; \\
 q_4 &= \sum_{i=1}^6 (x_i^2 - y_i^2); & q_5 &= \frac{1}{\sqrt{3}} \sum_{i=1}^6 (2z_i^2 - x_i^2 - y_i^2).
 \end{aligned}
 \tag{1}$$

The correlation between two quadrupole moments  $q$  and  $q'$  at different sites is given by

$$C = \frac{3}{16(b^2 - a^2)^2} (q_1 q'_1 + q_2 q'_2 + q_3 q'_3 + q_4 q'_4 + q_5 q'_5),
 \tag{2}$$

where  $a$  and  $b$  are the average length of short and long bonds in JT octahedra. In our normalization we used values of  $a = 1.94 \text{ \AA}$  and  $b = 2.16 \text{ \AA}$  as obtained previously by diffraction methods [12,17,20]. We also define a normalized magnitude for the quadrupole moment on a single site as

$$P^2 = \frac{3}{16(b^2 - a^2)^2} \left( \sum_{j=1}^5 q_j^2 \right),
 \tag{3}$$

so that a JT-distorted octahedron with bond lengths  $a$  and  $b$  will have a magnitude  $P \approx 1$ .

For octahedra with these bond lengths, the correlation factor  $C$  has values of  $+1$  for alignment (long bonds parallel) and  $-1/2$  for antialignment (long bonds perpendicular), and so is asymmetric by definition. Two other factors in the  $\text{LaMnO}_3$  system also make this correlation function asymmetric. In the low-temperature ordered form, the long axes of all octahedra lie in the  $xy$  plane and so the  $q_5$  component tends to be negative for all octahedra. Also,

the octahedra are tilted so that the long axes of adjacent octahedra are not exactly perpendicular. Both factors produce a positive bias on  $C$ . We therefore define a symmetrized correlation  $C'$  by subtracting from each individual quadrupole moment  $q$  [Eq. (1)], the average quadrupole moment  $\langle q \rangle$  for all octahedra in the model.  $C'$  lies approximately in the range

$$-1 < C' < +1,
 \tag{4}$$

where  $+1$  signifies alignment and  $-1$  antialignment.

Since in low-temperature, ordered  $\text{LaMnO}_3$ , the octahedra are ordered in the  $xy$  plane, we specifically consider the correlation in this plane, which we will call  $C'_{xy}$ . For each octahedron, we obtain its correlation  $C'_{xy}$  with its nearest-neighbor octahedra (those with which it shares a vertex) in the  $xy$  plane, with its second-nearest neighbors, and so on. We examine the distribution of these correlations for all octahedra in each model, from first neighbors out to tenth. In the fully ordered structure we expect the distribution of  $C'_{xy}$  for odd neighbors to peak around  $-1$ , and for even neighbors to peak around  $+1$ .

In Fig. 3 we show the distributions of  $C'_{xy}$  at several temperatures. At 300 K, the distributions for all odd neighbors are peaked around  $C'_{xy} \approx -1$ , and those for even neighbors are peaked around  $C'_{xy} \approx +1$ . At 700 K (just below the transition) the peaks have moved closer together and are broader. At 750 K (just above the transition) and 1050 K, the distributions for odd and even neighbors are almost superimposed on each other with mean correlations close to zero. At first sight it appears that all ordering is lost at high temperatures, despite the persistence of the JT distortion in each octahedron individually.

We examine the transition in more detail by extracting the mean value of  $C'_{xy}$  for each set of neighbors (first, second, third, and so on). At 300 K, the correlation is equally strong for all neighbors; odd neighbors (from 1st to 9th) are strongly anticorrelated, with  $\langle C'_{xy} \rangle$  close to  $-1$ , and even neighbors (from 2nd to 10th) are strongly correlated. At higher temperatures, however, a different pattern emerges. First,  $\langle C'_{xy} \rangle$  for first neighbors is more negative than  $\langle C'_{xy} \rangle$  for odd neighbors at longer range, indicating a stronger anticorrelation of first neighbors. As first neighbors share one oxygen atom in common in an  $\text{Mn}_A\text{-O-Mn}_B$  bridge, if the  $\text{Mn}_A\text{-O}$  distance is shorter it is intrinsically more likely that the  $\text{O-Mn}_B$  distance is longer. This also is in agreement with the observation of Qiu *et al.* [20] that small domains of order similar to the low-temperature ordered structure persist above the phase transition. More surprisingly, long-range ordering is not completely lost even at very high temperatures; an alternation in  $\langle C'_{xy} \rangle$  between odd and even neighbors is visible even at the highest temperatures, although the magnitude is quite small (at 1050 K,  $-0.011 < \langle C'_{xy} \rangle < 0.019$ , i.e., less than  $1/50$  of that seen at low temperature).

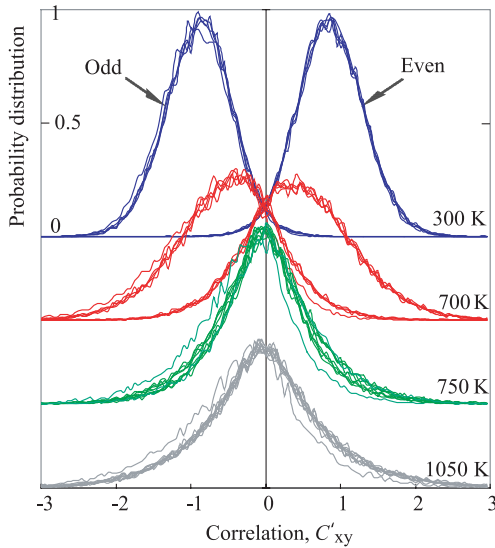


FIG. 3 (color online). Distribution of  $xy$ -plane correlation  $C'_{xy}$  at 300, 700, 750, and 1050 K. Below the JT transition the distributions for odd and even neighbors are quite distinct, while above the transition the distributions are almost superimposed.

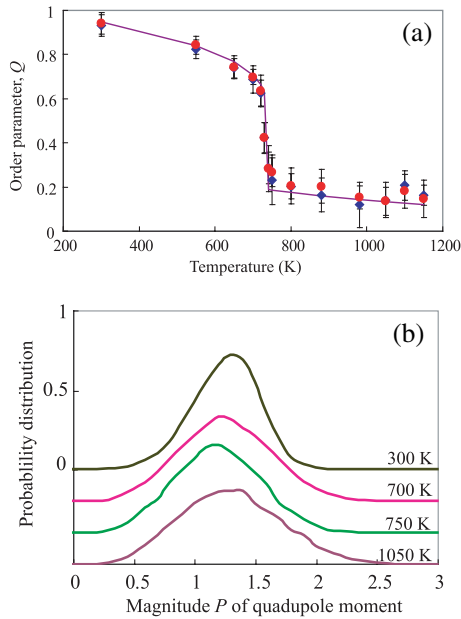


FIG. 4 (color online). (a) Order parameter  $Q$  vs temperature. Red (dark gray) and blue (gray) dots are determined from even and odd neighbors, respectively. (b) Probability distribution of quadrupole magnitudes,  $P$ , at selected temperatures.

From the behavior of the mean correlation, we obtain an order parameter  $Q$  describing long-range quadrupolar ordering. If the ordering on a site is proportional to the order parameter, then the correlation between sites is proportional to  $Q^2$ . Thus we estimate  $Q$  as  $\sqrt{|\langle C'_{xy} \rangle|}$  for neighbors, in the  $xy$  plane, at long range (i.e., not including first neighbors). In Fig. 4(a) we show this order parameter for all temperatures. We observe strong long-range order at lower temperatures and weak but nonzero long-range ordering at high temperatures, with a sharp (first-order) transition between the two at around 730 K. This is very similar to the form of quadrupolar ordering transition for  $S = \frac{3}{2}$  Ising systems studied by Sivardière and Blume [29]. The distribution of magnitudes  $P$  [Eq. (3)] of individual quadrupole moments of octahedra [Fig. 4(b)] shows that the full amplitude JT distortions persist up to the highest temperatures studied, consistent with earlier observations [20,21], and the drop in  $Q$  at high temperatures is due to a change in ordering, not to a loss of JT distortion on individual sites. It might appear disconcerting that the order parameter does not go to zero at the phase transition, but this is known to occur in quadrupolar systems. The existence of a field that couples to the order parameter (for example, an external magnetic field in a ferromagnet) will guarantee that the order parameter never goes to zero, and therefore destroys the critical point when the transition is second order. For quadrupolar ordering in, say, a spin  $S = 1$  system, the field that couples to the order parameter  $Q$  is a crystal field term like  $DS_z^2$ , where  $S_z$  is the  $z$  component

of the spin. A first-order phase transition can then occur where  $Q$  jumps at the transition and then has a tail at high temperatures [29]. In this case the field that couples to  $Q$  is generated internally by strain in the sample. Here we extract the order parameter directly from the PDF measurement bypassing the need to write down a Hamiltonian for the system.

Our results suggest the correlation of quadrupole distortions is the correct microscopic order parameter to describe the Jahn-Teller phase transition in  $\text{LaMnO}_3$ . The integrated experiment and modeling approach developed in this work, which involves incorporating local stereochemical constraints on the scattering data using geometrical simulation, should prove to be of wide validity in manganites, cuprates, and other materials with coupled local Jahn-Teller distortions.

- [1] T. Egami *et al.*, *Underneath the Bragg Peaks: Structural Analysis of Complex Materials* (Pergamon, Elsevier, New York, 2003).
- [2] T. Saitoh *et al.*, Phys. Rev. B **62**, 1039 (2000).
- [3] *Colossal-Magnetoresistive Oxides* edited by Y. Tokura (Gordon and Breach, New York, 2000).
- [4] A. P. Ramirez, J. Phys. Condens. Matter **9**, 8171 (1997).
- [5] K. H. Ahn and A. J. Millis, Phys. Rev. B **58**, 3697 (1998).
- [6] H. A. Jahn *et al.*, Proc. R. Soc. A **161**, 220 (1937).
- [7] J. B. Goodenough, Phys. Rev. **100**, 564 (1955).
- [8] J. C. Loudon *et al.*, Phys. Rev. Lett. **94**, 097202 (2005).
- [9] G. C. Milward *et al.*, Nature (London) **433**, 607 (2005).
- [10] A. J. Millis, Phys. Rev. B **53**, 8434 (1996).
- [11] *Nanoscale Phase Separation and Colossal Magnetoresistance*, edited by E. Dagotto (Springer-Verlag, Berlin, 2003).
- [12] T. Proffen *et al.*, Phys. Rev. B **60**, 9973 (1999).
- [13] S. J. L. Billinge *et al.*, Phys. Rev. B **62**, 1203 (2000).
- [14] E. S. Božin *et al.*, Phys. Rev. Lett. **98**, 137203 (2007).
- [15] S. Fujita *et al.*, *Theory of High-Temperature Superconductivity* (Kluwer Academic Publishers, Dordrecht, The Netherlands, 2001).
- [16] T. Egami, J. Supercond. Novel Magnetism **19**, 203 (2006).
- [17] J. Rodríguez-Carvajal *et al.*, Phys. Rev. B **57**, R3189 (1998).
- [18] C. P. Adams *et al.*, Phys. Rev. Lett. **85**, 3954 (2000).
- [19] T. Chatterji *et al.*, Phys. Rev. B **68**, 052406 (2003).
- [20] X. Qiu *et al.*, Phys. Rev. Lett. **94**, 177203 (2005).
- [21] M. Sanchez *et al.*, Phys. Rev. Lett. **90**, 045503 (2003).
- [22] J.-S. Zhou *et al.*, Phys. Rev. B **60**, R15002 (1999).
- [23] A. Sartbaeva *et al.*, Phys. Rev. Lett. **97**, 065501 (2006).
- [24] A. Sartbaeva *et al.*, Nat. Mater. **5**, 962 (2006).
- [25] T. Proffen *et al.*, J. Appl. Crystallogr. **32**, 572 (1999).
- [26] R. L. McGreevy, Nucl. Instrum. Methods Phys. Res., Sect. A **354**, 1 (1995).
- [27] S. A. Wells *et al.*, J. Phys. Condens. Matter **14**, 4567 (2002).
- [28] S. A. Wells *et al.*, Phys. Biol. **2**, S127 (2005).
- [29] J. Sivardière *et al.*, Phys. Rev. B **5**, 1126 (1972).